Shock Waves (1997) 7: 127–133

Shock Waves

Wave pattern characteristics of a two-phase nozzle flow by shock propagation

Q. S. Wu[1], **D. Z. Wang**[1] , **Y. H. Xu**[1], **B.Y. Wang**[2]

[1] Department of Mechanics, University of Science and Technology of China, Hefei 230026, People's Republic of China
[2] Institute of Mechanics, Chinese Academy of Sciences, Beijing 100080, People's Republic of China

Received 14 June 1996 / Accepted 19 October 1996

Abstract. In this paper, the wave pattern characteristics of shock-induced two-phase nozzle flows with the quiescent or moving dusty gas ahead of the incident-shock front has been investigated by using high-resolution numerical method. As compared with the corresponding results in single-phase nozzle flows of the pure gas, obvious differences between these two kinds of flows can be obtained.

Key words: Wave pattern, Shock propagation, Dusty gas, Two-phase flow, Convergent-divergent nozzle, Numerical analysis

1 Introduction

Investigation of the behavior of shock propagation in ducts with variable area, especially in convergent-divergent nozzles, is important in a range of practical applications such as analysis of the unsteady starting process of single- or double-driver shock tunnels. For the former, the gas in the nozzle ahead of the incident shock wave is quiescent while for the latter, it is moving. Since the 1960's many researchers have experimentally and numerically studied the features of shock-wave propagation in nozzles (Smith 1966; Amann 1969; Kashimura et al. 1986; Prodromou et al. 1991). However, only the simple case, in which the working medium is a pure gas and it is quiescent ahead of the incident shock wave, was considered. For the quiescent dusty gas and moving pure or dusty gases ahead of the shock front, studies remain to be carried out.

In this paper, the wave pattern characteristics of shock propagation along convergent-divergent nozzles are given on the basis of the simplified model of quasi-one-dimensional unsteady flow. The shock-induced two-phase nozzle flows in the quiescent or moving dusty gas ahead of the shock front are obtained by using high-resolution numerical methods–GRP scheme (Ben-Artzi and Falcovitz 1986) and NND-4 scheme (Zhang and Li 1992). As compared with the corresponding results in single-phase nozzle flows of the pure gas, obvious differences between these two kinds of flows can be seen. The basic phenomena and features of the two-phase nozzle flows by shock propagation are discussed in detail.

Correspondence to: B. Y. Wang

2 Physical model and governing equations

Suppose that the dusty gas is a dilute suspension of gas-particle mixture and the general assumptions suitable for this two-phase flow system are adapted (Crow 1982): (1) The particle phase can be regarded as continuous medium and the two-continuum model is employed for the flow system; (2) The gas phase is a compressible and perfect gas, whose viscosity and thermal conductivity are neglected except for the interactions between the gas and particles; (3) The particle phase consists of inert particles of uniform rigid spheres without Brownian motion and internal temperature gradient; (4) The volume fraction of particles is small enough to ignor the mutual interactions and partial pressure due to particle contribution; (5) There are momentum and energy (but no mass) exchanges between the two phases through interphase force and heat transfer; (6) The only force exerted on the particle is viscous drag. The other forces (pressure gradient force, Basselt force, virtual mass force, gravity force and lift force *etc.*) are neglected because they are much smaller than the friction force. Besides, suppose that the length-to-diameter (or width) ratio of the duct is large and the area-change rate in ducts is slow enough so that the nozzle flows can be approximately regarded as quasi-one-dimensional flows. Based on these assumptions above, we present the following governing equations for quasi-one-dimensional unsteady two-phase flows (Wang and Wu 1991)

$$\frac{\partial U}{\partial t} + \frac{1}{A}\frac{\partial AF(U)}{\partial x} + \frac{\partial G(U)}{\partial x} = H(U) \tag{1}$$

where

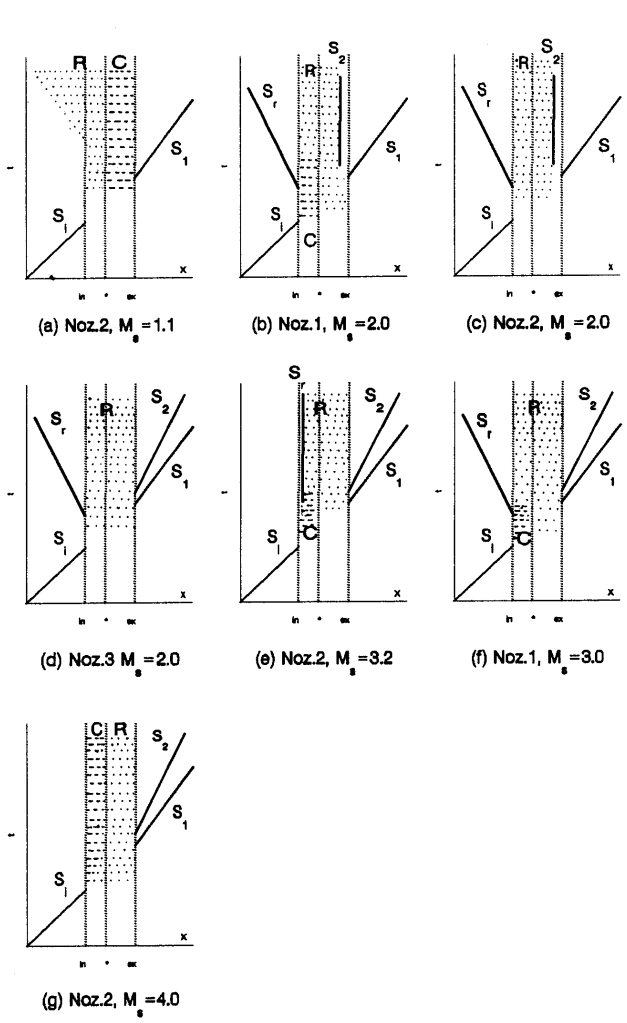

Fig. 1A. Wave patterns for a quiescent pure gas ahead of a shock

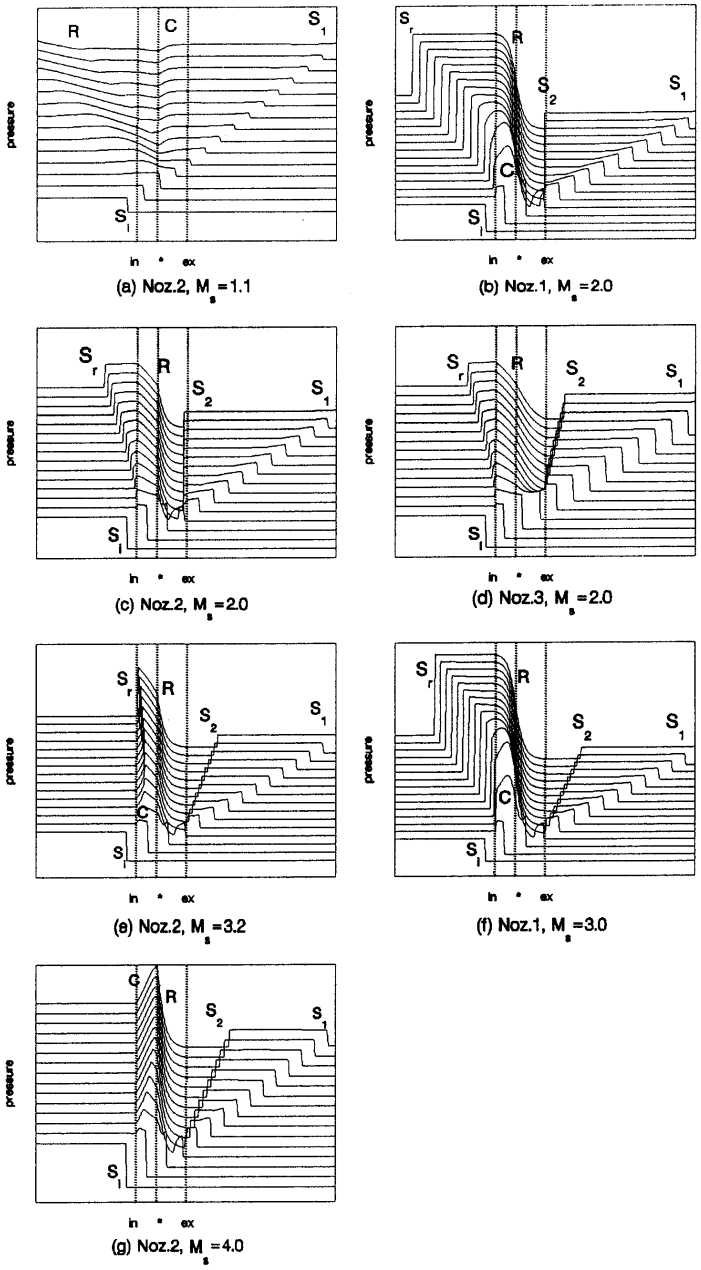

Fig. 1B. Pressure distributions at successive instants of time corresponding to wave patterns in Fig. 1A

$$U = \begin{pmatrix} \rho_g \\ \rho_g u_g \\ \rho_g(C_v T_g + \frac{u_g^2}{2}) \\ \rho_p \\ \rho_p u_p \\ \rho_p(C_m T_p + \frac{u_p^2}{2}) \end{pmatrix}, F(U) = \begin{pmatrix} \rho_g u_g \\ \rho_g u_g^2 \\ \rho_g u_g(C_p T_g + \frac{u_g^2}{2}) \\ \rho_p u_p \\ \rho_p u_p^2 \\ \rho_p u_p(C_m T_p + \frac{u_p^2}{2}) \end{pmatrix}$$

$$G(U) = \begin{pmatrix} 0 \\ p \\ 0 \\ 0 \\ 0 \\ 0 \end{pmatrix}, H(U) = \begin{pmatrix} 0 \\ -\rho_p D/m \\ -\rho_p(u_p D + Q)/m \\ 0 \\ \rho_p D/m \\ \rho_p(u_p D + Q)/m \end{pmatrix}$$

Here x, t and A stand for the space coordinate, time coordinate and duct-section area; ρ, T and u are the density, temperature and velocity (the subscripts g and p refer to the gas and particle phases); p is the gas pressure; C_m is the particle heat capacity; C_v and C_p are the gas specific heats respectively at constant volume and constant pressure; m, D and Q stand for the mass, drag and heat transfer of a single particle. In order to close Equation system (1), it is necessary to add the state equation of gas and the empirical relationships for D and Q which are

$$p = \rho_g R T_g \tag{2}$$

$$D = 0.125\pi d^2 \rho_g (u_g - u_p)|u_g - u_p|(0.48 + 28Re^{-0.85}) \tag{3}$$

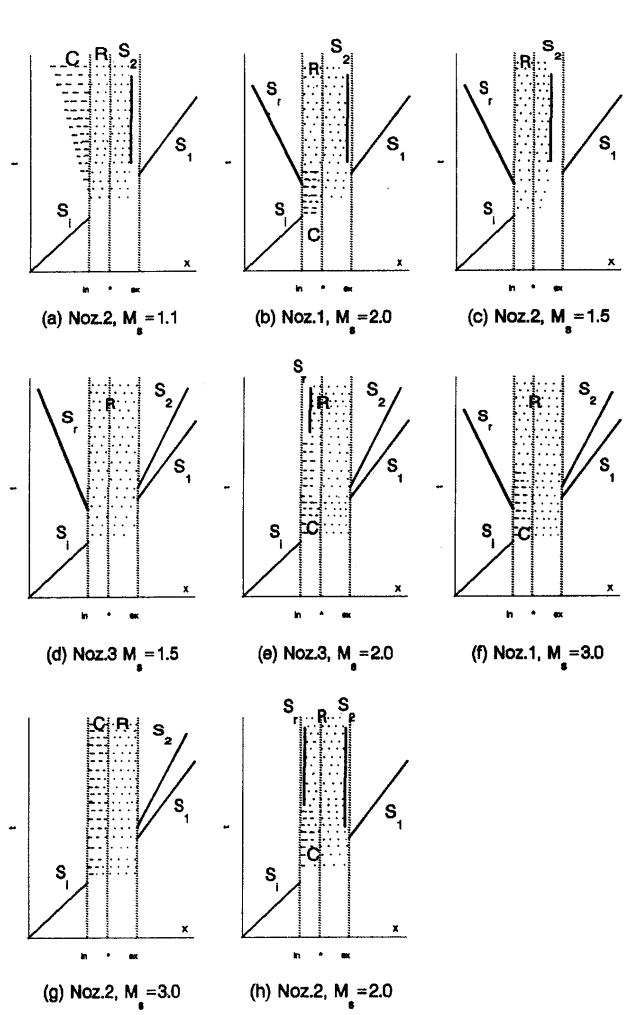

Fig. 2A. Wave patterns for a pure gas with a subsonic flow ahead of a shock ($M_{f^*} = 0.99$)

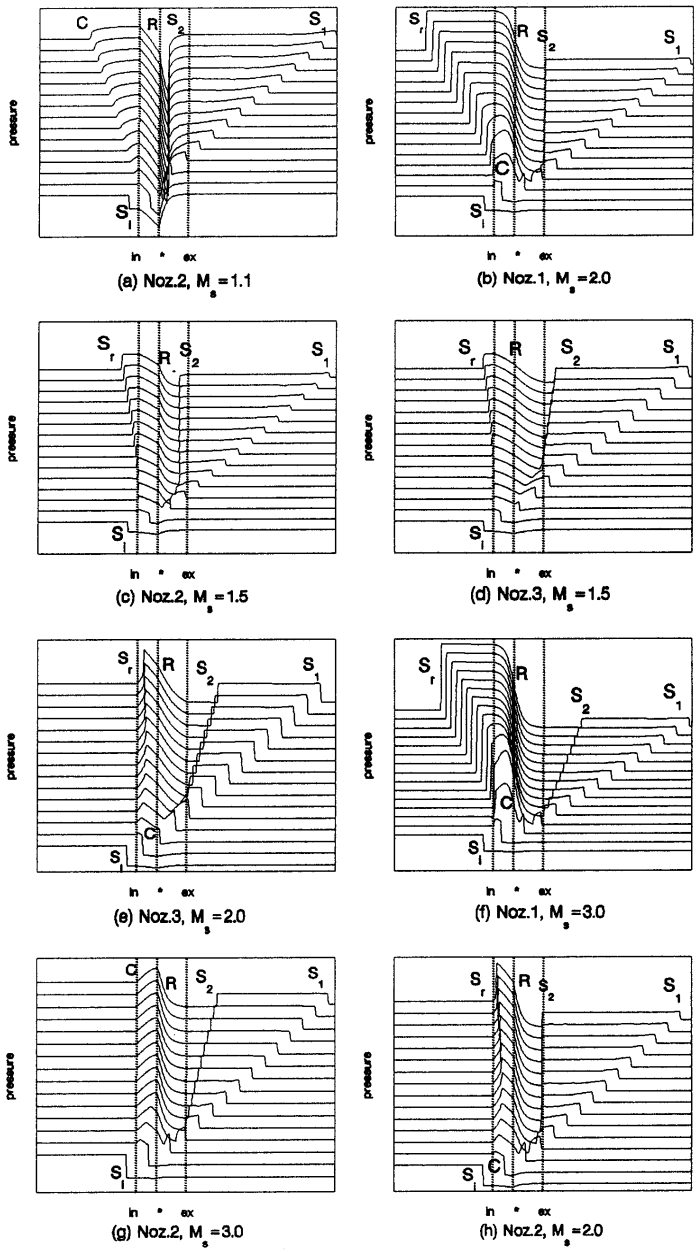

Fig. 2B. Pressure distributions at successive instants of time corresponding to wave patterns in Fig. 2A

$$Q = \pi d\mu C_p Pr^{-1}(T_g - T_p)(2.0 + 0.6Pr^{1/3}Re^{1/2}) \tag{4}$$

where R, Pr and μ are the gas constant, Prandtl number and viscosity coefficient respectively; d is the particle diameter; $Re = \rho_g|u_g - u_p|d/\mu$ is the slip Reynolds number. We consider the problem of dusty-gas shock waves propagating along a convergent-divergent nozzle with the given shape:

$$A = \begin{cases} A_{in} & x_{min} \le x \le x_{in} \\ A_* + (A_{in} - A_*)(\frac{x - x_*}{x_{in} - x_*})^2 & x_{in} < x \le x_* \\ A_* + (A_{ex} - A_*)(\frac{x - x_*}{x_{ex} - x_*})^2 & x_* < x \le x_{ex} \\ A_{ex} & x_{ex} < x \le x_{max} \end{cases} \tag{5}$$

where A_{in}, A_* and A_{ex} are the entrance, throat and exit areas of nozzle. The shape parameters are given as follows: $A_{in}/A_* = 4.0, 1.2, 1.2$ and $A_{ex}/A_* = 8.0, 8.0, 2.0$ respectively for the nozzle No. 1, 2, 3. We are interested in the wave patterns over the convergent-divergent part of duct sections. When the uniform parts of duct sections are long enough so that there is no reflection at the ends. This fact can be taken as numerical boundary conditions.

3 Numerical method

The operator-splitting technique is applied to deal with the coupling effects between the gas and particle phases. The Equation

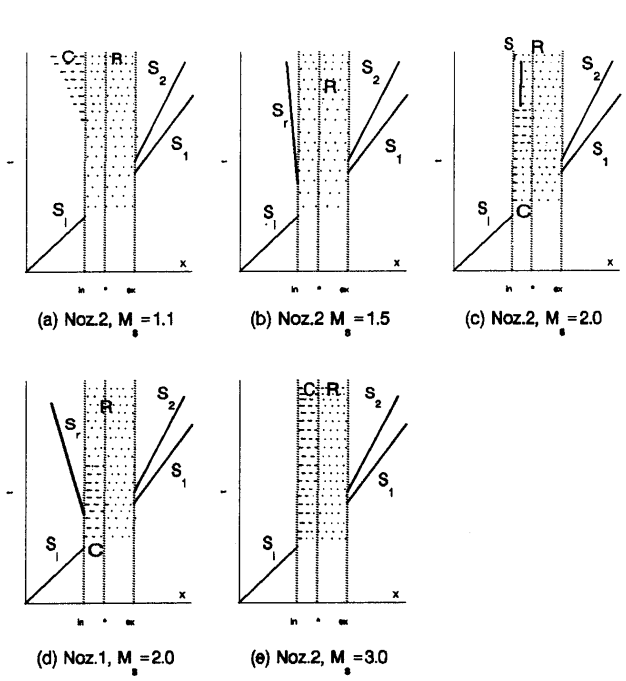

Fig. 3A. Wave patterns for a pure gas with a subsonic-supersonic flow ahead of a shock ($M_{r^*} = 1.0$)

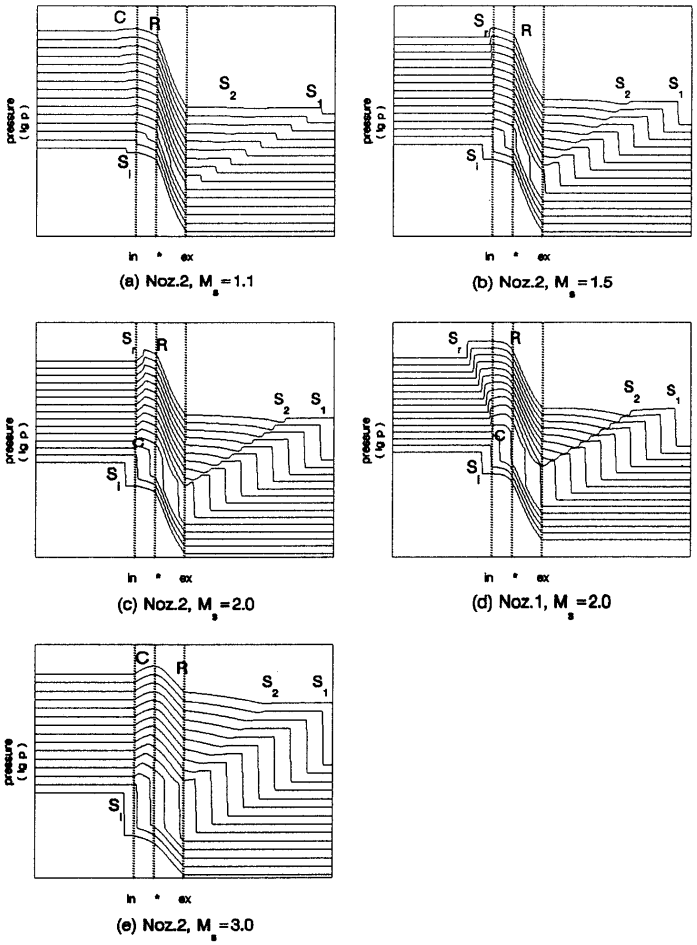

Fig. 3B. Pressure distributions at successive instants of time corresponding to wave patterns in Fig. 3A

system (1) is decomposed into the following two systems:

$$\frac{\partial U}{\partial t} + \frac{1}{A}\frac{\partial AF(U)}{\partial x} + \frac{\partial G(U)}{\partial x} = 0 \tag{6}$$

$$\frac{dU}{dt} = H(U) \tag{7}$$

In this way, there are interphase interaction terms only in Equation system (7) and the equations for the gas and particle phases in Equation system (6) are uncoupled. We construct the GRP scheme to solve the gas-phase equations of hyperbolic type:

$$\begin{aligned}\widetilde{U}_i^{n+1} = U_i^n &- \frac{\Delta t}{\Delta V_i}[A_{i+1/2}F(U)_{i+1/2}^{n+1/2} \\ &- A_{i-1/2}F(U)_{i-1/2}^{n+1/2}] \\ &- \frac{\Delta t}{\Delta x}[G(U)_{i+1/2}^{n+1/2} - G(U)_{i-1/2}^{n+1/2}]\end{aligned} \tag{8}$$

where

$$\Delta V_i = \int_{x_{i-1/2}}^{x_{i+1/2}} A(x)dx$$

$$F(U)_{i\pm1/2}^{n+1/2} = F(U_{i\pm1/2}^n) + \frac{\Delta t}{2}(\frac{\partial F}{\partial U})_{i\pm1/2}^n(\frac{\partial U}{\partial t})_{i\pm1/2}^n$$

$$G(U)_{i\pm1/2}^{n+1/2} = G(U_{i\pm1/2}^n) + \frac{\Delta t}{2}(\frac{\partial G}{\partial U})_{i\pm1/2}^n(\frac{\partial U}{\partial t})_{i\pm1/2}^n$$

Here $U_{i\pm1/2}^n$ and $(\partial U/\partial t)_{i\pm1/2}^n$ denote the solution to generalized Riemann problem and its time derivative at the cell boundaries $x_{i\pm1/2}$. For the particle-phase equations of parabolic type, we employ the two-step NND-4 scheme and have the following difference formulae:

$$\widetilde{\widetilde{U}}_i^{n+1} = U_i^n - \frac{1}{A_i}\frac{\Delta t}{\Delta x}(W_{i+1/2}^n - W_{i-1/2}^n) \tag{9}$$

$$\widetilde{U}_i^{n+1} = \frac{1}{2}[U_i^n + \widetilde{\widetilde{U}}_i^{n+1} - \frac{1}{A_i}\frac{\Delta t}{\Delta x}(\widetilde{\widetilde{W}}_{i+1/2}^{n+1} - \widetilde{\widetilde{W}}_{i-1/2}^{n+1})] \tag{10}$$

Due to the fact that the eigenvalues are all positive (denoted with the superscript +), the flux function W is defined as

$$W_{i+1/2}^n = (AF)_{i+1/2,L}^+$$

$$\begin{aligned}(AF)_{i+1/2,L}^+ = (AF)_i^+ \\ + \frac{1}{2}\text{minmod}[\Delta(AF)_{i-1/2}^+, \Delta(AF)_{i+1/2}^+]\end{aligned}$$

$$\Delta(AF)_{i+1/2}^+ = (AF)_{i+1}^+ - (AF)_i^+$$

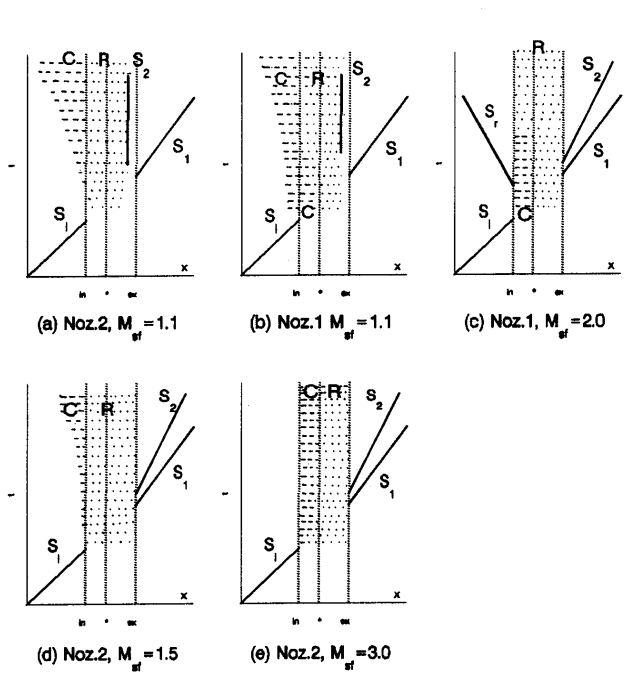

Fig. 4A. Wave patterns for a quiescent dusty gas ahead of a shock

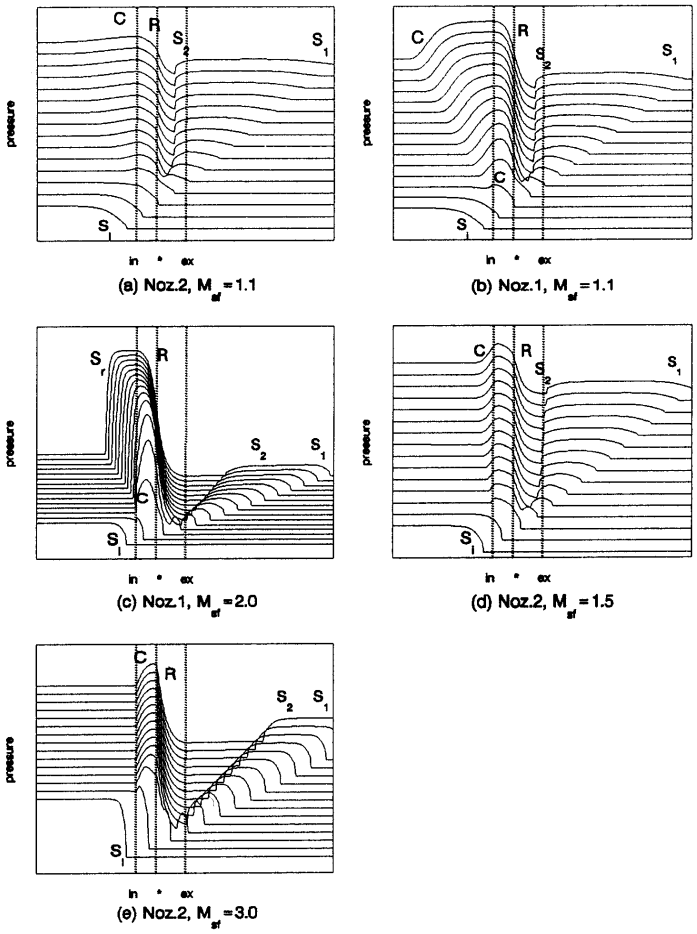

Fig. 4B. Pressure distributions at successive instants of time corresponding to wave patterns in Fig. 4A

where

$$\text{minmod}(x, y) = Sign(x) \cdot \max[0, \min(|x|, Sign(x) \cdot y)]$$

For every time-level t_n, by using this procedure, the solutions to the homogeneous partial differential equations, Eq. (6), $\widetilde{U}_i^{n+1}$ can be obtained. Then the ordinary differential equations, Eq. (7), are solved by the predictor-corrector method and the homogeneous solutions are considered as their initial conditions:

$$\overline{U}_i^{n+1} = \widetilde{U}_i^{n+1} + \Delta t H(\widetilde{U}_i^{n+1}) \tag{11}$$

$$U_i^{n+1} = \widetilde{U}_i^{n+1} + \frac{\Delta t}{2}[H(\widetilde{U}_i^{n+1}) + H(\overline{U}_i^{n+1})] \tag{12}$$

where U_i^{n+1} are the desired solutions at the time-level t_{n+1}. Obviously, all the three difference schemes presented above have second-order accuracy in space and time.

4 Numerical results and discussion

In order to perform comparative studies, six cases are considered: Cases 1 to 3 correspond to the pure gas and Cases 4 to 6 to the dusty gas. In computation, we take the particle parameters as follows: the particle diameter $d = 10\mu m$, the loading ratio $\alpha = \rho_p/\rho_g = 1.0$, the ratio of specific heats $\beta = C_m/C_v = 1.0$, the material density of particles $\sigma_p = 2500\text{kg/m}^3$. Concerning the flow conditions ahead of the incident shock, Cases 1 and 4 are at a quiescent state, Cases 2 and 5 at a subsonic state, and Cases 3 and 6 at a subsonic-supersonic state. The possible wave patterns for Cases 1 to 6, which are obtained by changing the incident-shock Mach number and the nozzle-shape parameters, are schematically shown in Figs. 1A to 6A. In these figures, M_{1^*} refers to the pre-shock-flow Mach number at the throat and the subscript e to the dusty gas at equilibrium. The corresponding pressure distributions at successive instants of time are shown in Figs. 1B to 6B. Because the maximum-to-minimum pressure ratio is very large for the Cases 3 and 6, the pressure values indicated in the vertical axis are taken logarithm to the base 10 in order to show the shock waves clearly. In these figures S_i, S_1, S_2, S_r, C and R refer to the incident shock, the transmitted (primary) shock, the secondary shock, the reflected shock, the compressible wave and the rarefaction wave, respectively. The calculation results indicate that there are some similar features in the nozzle flows for the pure gas and dusty gas. In the nozzle divergent zone, the flow ahead of the secondary shock wave is expansive provided that the induced flow behind the nozzle throat is supersonic. In the

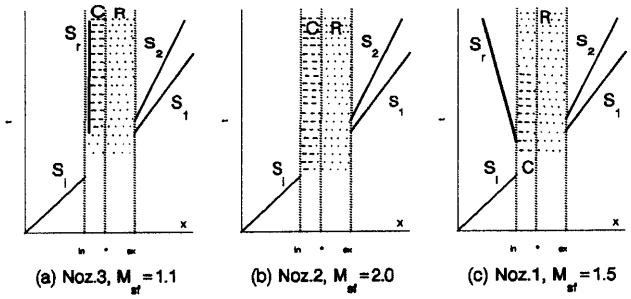

Fig. 5A. Wave patterns for a dusty gas with an equilibrium subsonic flow ahead of a shock ($M_{fe^*} = 0.99$)

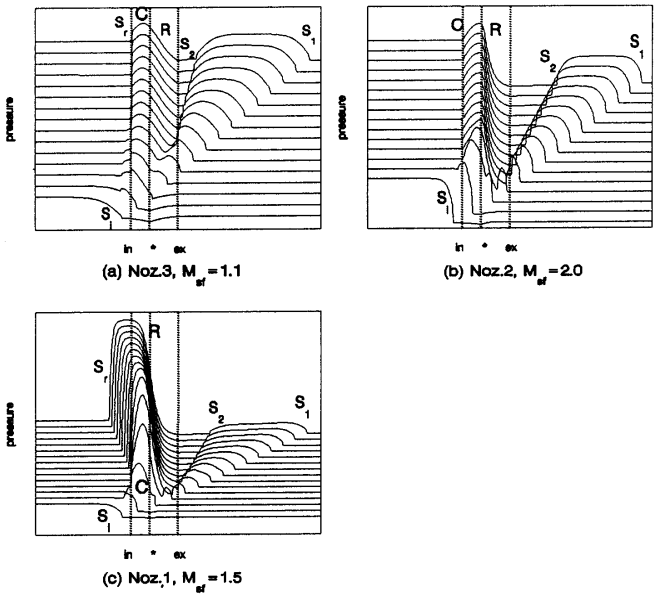

Fig. 5B. Pressure distributions at successive instants of time corresponding to wave patterns in Fig. 5A

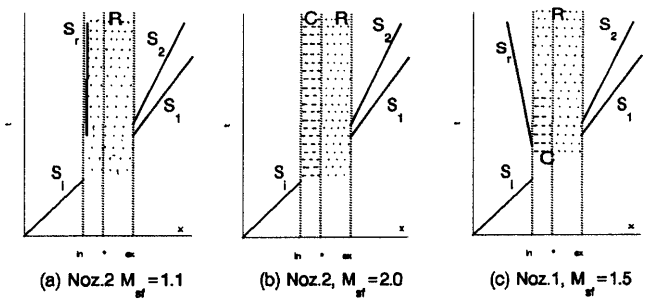

Fig. 6A. Wave patterns for a dusty gas with an equilibrium subsonic-supersonic flow ahead of a shock ($M_{fe^*} = 1.0$)

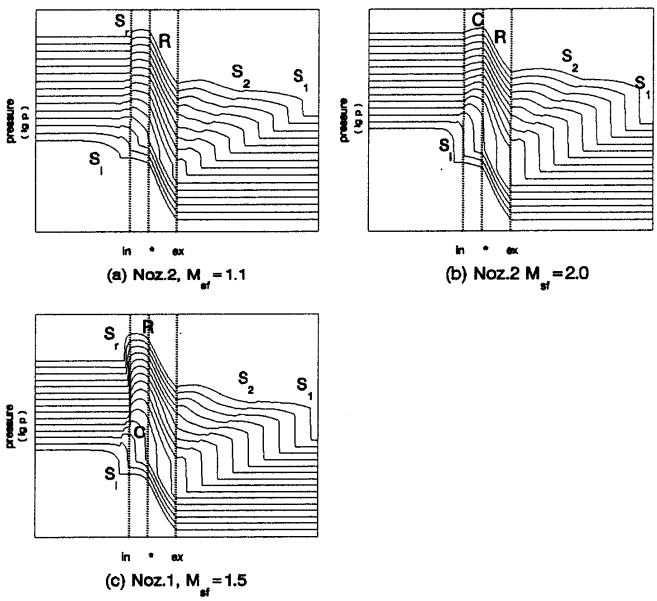

Fig. 6B. Pressure distributions at successive instants of time corresponding to wave patterns in Fig. 6A

nozzle convergent zone, the flow is all expansive in the small convergent-ratio or weak incident-shock cases. When the convergent ratio is large or the incident shock is strong, the flow is firstly compressible and then gradually changed to expansive. When the incident shock is very strong, the flow is all compressible. However, comparing Figs. 1, 2, 3 for the pure gas with Figs. 4, 5, 6 for the dusty gas, obvious differences can be found between these two kinds of flows:

(1) As long as the nozzle-throat flow induced by the incident shock wave is sonic or supersonic for which the flow is expansible after the throat, the secondary shock will be produced behind the primary shock. Depending on the shock strength and the convergent-divergent ratio of the nozzle, the secondary shock either stops in the divergent zone or propagates downstream. However, the incident frozen-shock Mach number M_{sf} in the dusty gas is less than the incident shock Mach number M_s in the pure gas for the same nozzle and the same wave-pattern structures. This is because that the wave-pattern structures depend on the drive-pressure ratio for the same nozzle. Under the same drive-pressure ratio, M_{sf} is less than M_s due to the interphase relaxation behind the shock front.

(2) When the incident shock wave enters the nozzle, whether there is reflection (and of what kind) depend on the nozzle shape and the incident-shock strength. In Case 4 for the dusty gas at the quiescent state ahead of the incident shock, the possibility to reflect compressible waves is higher than shock waves. However, in the other five cases, the shock wave will be reflected except when the incident shock is very weak or strong. For a very weak incident-shock (in our cases, $M_s = 1.1$), either rarefaction or compressible waves will be reflected. For a stronger incident shock (in our cases, $M_s = 2.0$ – 3.0) entering into a moving gas or for a very strong incident shock (in our cases, $M_s > 3.0$) entering into a quiescent gas, there will be no wave reflection at all. However, for the dusty gas, there are more cases reflecting compressible waves compared with those reflecting shock waves. This is because that the equilibrium drive pressure behind the relaxation zone in the dusty gas is higher than the drive pressure in the pure gas. Therefore, it is more difficult to form the reflected shock wave.

(3) The number of possible wave patterns are 7, 8, 5 for Cases 1, 2, 3 and 5, 3, 3 for Cases 4, 5, 6. In other words, there are likely less wave patterns in the dusty gas than those in the pure gas. By comparison of pressure distributions, the relaxation features behind the incident shock wave have been obviously indicated for the dusty gas. In the pure-gas case, the pressure monotonically decreases behind the shock wave front. But in the dusty-gas case, it continuously increases up to a maximum value and then decreases. This is because that there are interactions between the gas and particles. From the pressure distribution in Fig. 6B, it can be seen that the secondary shock is very weak and nearly dispersed due to the particle presence.

(4) Now consider the effects of motion state ahead of the incident shock wave on the wave pattern characteristics. For the pure gas, the wave-pattern structures and pressure-distribution features are approximately the same in the quiescent and subsonic states ahead of the incident shock. However, for the same wave pattern, the corresponding incident-shock Mach number M_s is less when the flow ahead of the incident shock is subsonic. If the steady nozzle flow ahead of the incident shock is subsonic-supersonic, the secondary shock does not stop in the nozzle divergent zone and the total number of wave patterns is less than that in the cases where there is no flow or subsonic flow ahead of the incident shock. For the dusty gas, the wave patterns are approximately the same when the flow ahead of the incident shock is subsonic or subsonic-supersonic. The secondary shock wave may not stop in the nozzle divergent zone, but the reflected shock wave may stop in the nozzle convergent zone.

5 Concluding remarks

The results of numerical investigation indicate that the features of shock propagation in a dusty gas along convergent-divergent nozzles are different from those in a pure gas. For the same nozzles and the same incident shock strength ($M_{sf} = M_s$) there are different wave pattern structures. For the same induced wave pattern the necessary incident shock strength and the nozzle parameter are different. These differences change with the quiescent or moving state of the medium ahead of the incident shock. They are produced by the interphase relaxation effects behind the shock waves and the interactions between the incident shock wave and the steady equiliblium two-phase flow ahead of the shock front.

Acknowledgements. The financial support provided by the National Natural Science Foundation of China is gratefully acknowledged.

References

Amann HO (1969) Experimental study of starting process in a reflection nozzle. Phys Fluids 12:150–153

Ben-Artzi M, Falcovitz J (1986) An upwind second-order scheme for compressible duct flows. SIAM J Sci Stat Comp 7:744–768

Crow CT (1982) Review–numerical models for dilute gas-particle flows. J of Fluid Eng 194:297–303

Kashimura H, Iwata N, Nishida M (1986) Numerical analysis of the wave propagation in a duct with an area change by random choice method. Bulletin JSME 29:1440–1445

Prodromou P, Hillier R (1991) Computation of unsteady nozzle flows. In: Takayama K (ed) Proc 18th Int Symp on Shock Waves, Vol 2 Sendai:1113–1118

Smith CE (1966) The starting process in a hypersonic nozzle. J Fluid Mech 24:625–640

Wang BY, Wu QS (1991) Numerical investigation of dusty gas shock wave propagation along a variable cross-section channel. In: Takayama K (ed) Proc 18th Int Symp on Shock Waves, Vol. 1, Sendai: 521–526

Zhang HX, Li ZW (1992) Numerical simulation of hypersonic laminar wake flow. Acta Mechanica Sinica 24:389–399